Tailoring Galvanic Replacement Reaction for the Preparation of Pt/Ag Bimetallic Hollow Nanostructures with Controlled Number of Voids

Weiqing Zhang, Jizheng Yang, and Xianmao Lu*

Department of Chemical and Biomolecular Engineering, National University of Singapore, Singapore 117576

ABSTRACT

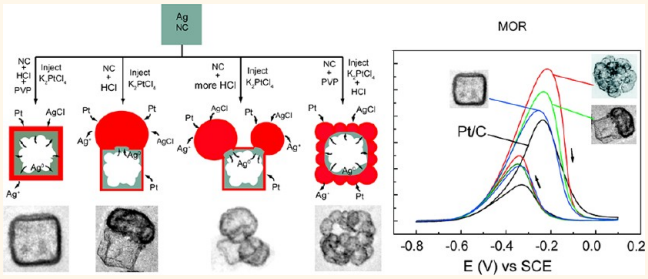

Here we report the synthesis of Pt/Ag bimetallic nanostructures with controlled number of void spaces *via* a tailored galvanic replacement reaction (GRR). Ag nanocubes (NCs) were employed as the template to react with Pt ions in the presence of HCl. The use of HCl in the GRR caused rapid precipitation of AgCl, which grew on the surface of Ag NCs and acted as a removable secondary template for the deposition of Pt. The number of nucleation sites for AgCl was tailored by controlling the amount of HCl added to the Ag NCs or by introducing PVP to the reaction. This strategy led to the formation of Pt/Ag hollow nanoboxes, dimers, multimers, or popcorn-shaped nanostructures consisting of one, two, or multiple hollow domains. Due to the presence of large void space and porous walls, these nanostructures exhibited high surface area and improved catalytic activity for methanol oxidation reaction.

KEYWORDS: galvanic replacement reaction · nanobox · heterodimer · nanopopcorn · methanol oxidation reaction

Galvanic replacement reaction (GRR) has emerged as a powerful synthetic approach for converting solid metal nanostructures into hollow ones that are advantageous in optical and catalytic properties.[1−4] Typically, GRR-based synthesis involves the use of metal nanostructures as sacrificial templates to react with ions of a more noble metal. Due to the difference in electrode potentials of the two metals, the nanostructured metal templates will be dissolved and the more noble metal ions will be reduced to elemental form, which subsequently deposits onto the surface of the templates.[5−7] Depending on a number of factors such as similarity in crystal structures, degree of lattice mismatch, and difference in metallic bonding strengths, a conformal or a nonconformal growth of the second metal may take place on the surface of the template to form a shell while the first metal is continuously consumed from the core. In the end, a structure with a hollow interior and a shell composed of either just the second metal or the alloy of both metals can be formed.

To date, a wide variety of hollow nanostructures including spherical nanoshells,[8] cubic nanoboxes,[9,10] nanocages,[7,11] hollow nanorods,[6] nanotubes,[12] nanorattles,[13] nanoframes,[14] and nanodendrites[15,16] composed of Au,[7,17] Pd,[18−20] and/or Pt[20−22] have been prepared *via* GRR using nanotemplates of Ag,[7,17] Cu,[18,20] or more reactive metals (*e.g.*, Zn or Mg[22,23]). These hollow nanostructures have found applications in areas including biomedical imaging,[24] photothermal cancer treatment,[4,25] drug delivery,[26] surface-enhanced Raman scattering,[27,28] and electrochemical catalysis.[29−31] In most cases, the shape of the hollow nanostructures obtained *via* GRR resembles that of the sacrificial templates. For instance, when Ag nanocubes (NCs) are used as the template to react with $HAuCl_4$, hollow Au/Ag nanoboxes can be prepared.[7] Novel structures such as nanobowls[32] or multiple-walled nanoshells[13] have also been synthesized, although complex templates are necessary for generating such structures. Here we show that by tuning the GRR between Ag NCs and K_2PtCl_4, Pt/Ag bimetallic hollow nanostructures with distinct shapes and tailored number of void zones can be readily obtained. Figure 1 illustrates the hollow nanostructures and their corresponding

* Address correspondence to chelxm@nus.edu.sg.

Received for review June 12, 2012 and accepted July 17, 2012.

Published online July 17, 2012
10.1021/nn302590k

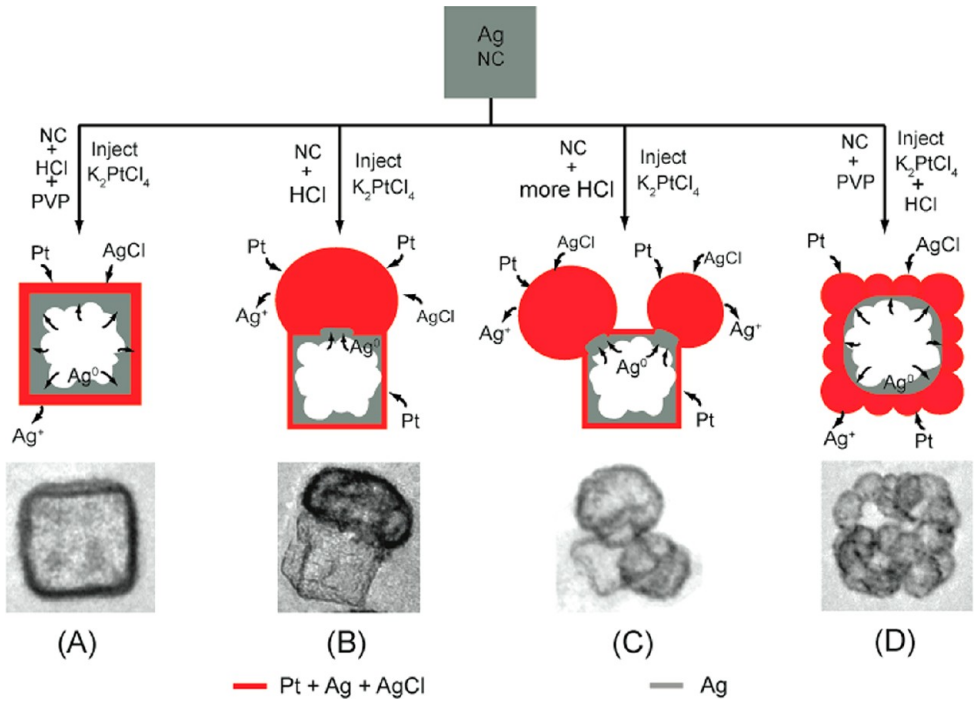

Figure 1. Illustration of the formation of Pt/Ag (A) nanobox, (B) heterodimer, (C) multimer, and (D) popcorn-shaped nanoparticle from the GRR between Ag NCs and K_2PtCl_4 in the presence of HCl.

reaction conditions (see Methods for experimental details). In the first case, both HCl and PVP are introduced into the dispersion of Ag NCs. After injecting K_2PtCl_4 solution, Pt/Ag nanoboxes with smooth and continuous walls are obtained (Figure 1A). However, if only HCl is added into the dispersion of Ag NCs before the injection of K_2PtCl_4, the reaction gives Pt/Ag heterodimers, a structure consisting of a hollow box with an attached particle (Figure 1B). At higher concentration of HCl, the number of attached particles on each hollow nanobox increases, leading to the formation of multimeric nanostructures (Figure 1C). If HCl is mixed with K_2PtCl_4 solution before it is reacted with Ag NCs, Pt/Ag hollow nanostructures consisting of multiple attached particles, namely, popcorn-shaped particles, are formed (Figure 1D). Subsequent washing with NaCl and $Fe(NO_3)_3$ solutions can further convert the attached solid particles into hollow ones. Compared with nanoboxes with single void interior, the dimeric, multimeric, and popcorn-shaped nanostructures consisting of two or more hollow domains within one particle show much increased surface area and should be beneficial to their catalytic applications.

RESULTS AND DISCUSSION

The formation of Pt/Ag dimeric, multimeric, and popcorn-shaped nanostructures in addition to simple nanoboxes is made possible by two reasons. First, we take the advantage of the undesirable byproduct, AgCl, of the reaction to direct the deposition of Pt. The GRR between Ag and K_2PtCl_4 generates AgCl, which has a low solubility in water and may precipitate out from the solution.[7,33] In this work, HCl is used to purposely facilitate the precipitation of AgCl, which subsequently grows on the surface of Ag NCs to form attached islands. With the progress of the reaction, the AgCl islands serve as *in situ* generated secondary templates for the deposition of Pt. Once the reaction completes, AgCl can be easily removed by washing with saturated NaCl solution to form void space. Second, the number of AgCl islands attached on each Ag NC is regulated by either adjusting the concentration of HCl or by adding PVP to the dispersion of Ag NCs. We found that while HCl at higher concentration leads to higher reaction kinetics and hence multiple attached islands on Ag NCs, the addition of PVP results in uniform coating of AgCl and thus smooth hollow nanoboxes. Together, these two mechanisms allow us to extend GRR to the preparation of more complex bimetallic nanostructures with tailored number of hollow domains.

Figure 2A shows the Pt/Ag nanoboxes with smooth and continuous walls prepared by adding 0.23 mL of HCl (10 mM) and 0.5 mL of PVP (100 mM) to the dispersion of 70 nm Ag NCs, followed by the injection of 0.5 mL of K_2PtCl_4 (5 mM) at 100 °C. The nanoboxes display a well-defined cubic shape with an average edge length of 75 nm and a wall thickness of ~10 nm. High-resolution transmission electron microscopy (HRTEM) image of the nanoboxes reveals porous but single-crystalline walls with lattice fringes corresponding to the (100) plane of Pt/Ag alloy (Figure S2A in the Supporting Information). The GRR between Ag nanostructures and Pt ions has been widely investigated for the preparation of Pt/Ag bimetallic structures,

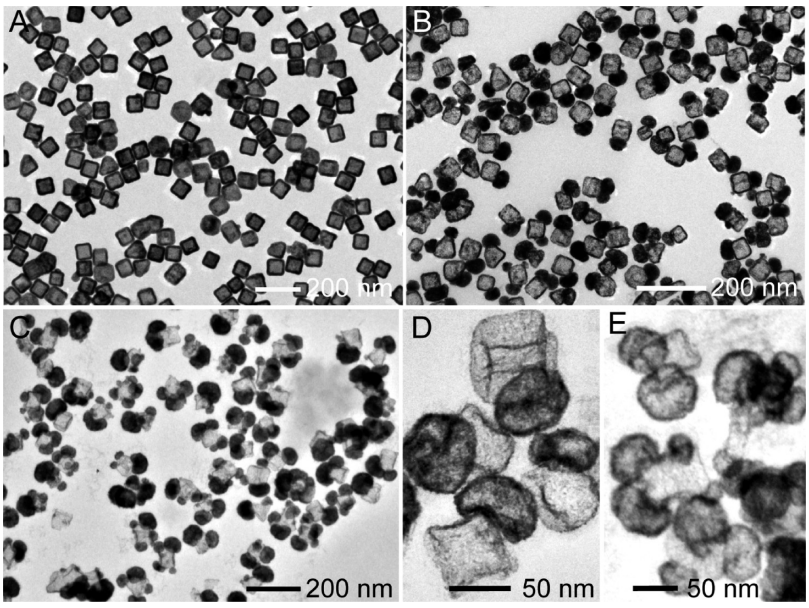

Figure 2. TEM images of (A) Pt/Ag nanoboxes, (B) Pt/Ag heterodimers, (C) Pt/Ag multimers. After washing with solutions of saturated NaCl and 50 mM $Fe(NO_3)_3$, the (B) dimers and (C) multimers were converted to nanostructures with (D) two or (E) multiple hollow domains, respectively.

although hollow nanoboxes with continuous and smooth walls have been scarcely observed.[5,31,34−36] For instance, Xia *et al.* employed Ag NCs to react with Na_2PtCl_4 to form nanoboxes.[19] In contrast to the Au/Ag system, where the reaction between Ag NCs and $HAuCl_4$ gives Au/Ag alloy nanoboxes with a smooth surface,[7] the Pt/Ag hollow nanostructures in their work displayed a rough surface decorated with Pt nanoparticles. The difficulty in forming Pt/Ag hollow nanostructures with smooth walls has been attributed to a number of reasons, including (1) the large lattice mismatch between Pt and Ag (4.3% for Au and 0.2% for Ag); (2) the difficulty in forming alloys between Pt and Ag—it has been shown that, even melted together, Pt and Ag would not be able to form alloy with Pt >5%;[19] and (3) the slower reaction rate between Pt ions and Ag atoms than that for the reaction between Au ions and Ag.[37] Interestingly, in our work, by adding HCl and PVP to the dispersion of Ag NCs before they were reacted with K_2PtCl_4, hollow Pt/Ag nanoboxes with smooth walls were readily obtained.

The reaction between Ag and K_2PtCl_4 is as follows: $2Ag + K_2PtCl_4 \rightarrow Pt + 2AgCl + 2KCl$. With the reduction of K_2PtCl_4, Pt is formed and deposited onto the surface of the Ag templates. As a byproduct of the reaction, AgCl is also generated. As mentioned earlier, due to the low solubility of AgCl in water (1.33×10^{-5} mol/L at 25 °C),[33] AgCl may precipitate out and interfere unfavorably with the deposition of Pt. To avoid the precipitation of AgCl, one may raise the reaction temperature to increase the solubility of AgCl (10 times higher at 100 °C). This method has proven to be effective for the reaction between $HAuCl_4$ and Ag nanostructures to form hollow Au/Ag nanostructures with smooth walls.[7]

Another approach is to add chemicals that react with AgCl to form soluble species. For example, Xu *et al.* used highly concentrated HCl (3 M) in the GRR between H_2PtCl_6 and porous Ag so that AgCl can be converted to soluble complex $AgCl_2^-$.[5] However, when HCl at low concentration (0.44 mM in our work) was used during the galvanic replacement reaction, one would expect that the precipitation of AgCl will occur at even lower concentration of Ag^+; and it is counterintuitive to obtain nanoboxes with smooth and continuous walls. Therefore, in our case, where both HCl and PVP were added to the dispersion of Ag NCs, the deposition of AgCl might take place evenly on the surface of Ag NCs. The presence of AgCl on the whole surface of the NCs facilitated the growth of a uniform layer of Pt. Although the reason is not clear yet, the use of AgCl for the growth of a uniform Pt layer on Ag has been previously reported. For instance, Ye *et al.*[38] found that while the GRR between Ag nanowires and H_2PtCl_6 led to the formation of aggregated Pt nanoparticles on the Ag surface, heteroepitaxial growth of a continuous Pt layer was achieved if Ag nanowires were treated with $FeCl_3$ solution to form a AgCl layer before the GRR. In another work, Lee *et al.* also employed AgCl nanocubes as removable templates for the growth of Pt, which eventually evolved into smooth Pt hollow nanoboxes.[9] In our work, the existence of AgCl in the walls of the resultant nanoboxes was confirmed from energy-dispersive X-ray spectroscopy (EDX). EDX line profile of the Pt/Ag nanoboxes shows that, in addition to Pt and Ag, strong signal from Cl is also revealed (Figure S2B). Since the samples were washed carefully before the EDX measurements, the existence of Cl cannot be solely attributed to surface-adsorbed species.

Therefore, an appreciable amount of AgCl is expected in the walls of the hollow nanoboxes. It should be noted that when the hollow nanoboxes were washed by saturated NaCl and $Fe(NO_3)_3$ solutions, the wall thickness decreased because of the removal of AgCl and Ag, respectively (Figure S2C). This is because saturated NaCl solution can form a soluble complex with AgCl,[7] while $Fe(NO_3)_3$ oxidizes Ag.[14] In addition to the effect of AgCl, suitable reaction kinetics may also contribute to the deposition of smooth Pt layer on the Ag NCs. Recently, El-Sayed *et al.* reported that Pt/Ag nanoboxes with porous continuous walls can be synthesized based on the GRR between Ag NCs and K_2PtCl_4.[37] In their study, K_2PtCl_4 at high concentration was used to achieve fast reaction at the initial stage, while a subsequent low reaction rate was attained by switching to K_2PtCl_4 at low concentration. The success of this strategy in facilitating the formation of Pt/Ag nanoboxes with smooth walls indicates the importance of the right reaction kinetics. Compared to the GRR between K_2PtCl_4 and Ag NCs without HCl, we found that the color change of the reaction from yellow to gray occurred much faster when HCl was added to the Ag NCs (20 *vs* 4 s), indicating higher reaction rate in the presence of HCl. The use of halide ions to promote GRR kinetics can be attributed to the enhanced surface diffusivity of Ag due to the strong coordination of halide ions to Ag^+.[39] Similar effect has been observed for the case of Pd. For instance, Zheng *et al.* found that, for the GRR between Pd nanocubes and $Pt(acac)_2$, the use of I^- may facilitate the out-diffusion of Pd for creating hollow Pt/Pd nanoboxes.[10] Xia *et al.* also employed Br^- for the preparation of Pt/Pd concave nanostructures.[21]

In addition to HCl, PVP also plays an important role in defining the morphology of the Pt/Ag nanostructures. PVP is often used as a shape and size control agent in nanostructure synthesis. When reactions similar to the synthesis of Pt/Ag nanoboxes were carried out without adding PVP (*i.e.*, following the reaction route in Figure 1B), heterodimers instead of nanoboxes were obtained. Figure 2B shows the dimeric nanoparticles prepared by adding 0.23 mL of 10 mM HCl into the dispersion of 50 nm Ag NCs (molar ratio of HCl/Ag = 2.75:1), followed by injecting 0.5 mL of K_2PtCl_4 solution (5 mM) at 100 °C. TEM of the as-prepared samples shows that each heterodimer is composed of two domains—a hollow nanobox with an attached solid particle. For most dimers, the solid particle is located at the corner of the nanoboxes, although some along the side have also been observed. The nanoboxes have an average edge length of 50 nm with a wall thickness of ~5 nm. The average size of the attached particles is 53 nm, close to that of the nanoboxes. We also found that the number of attached particles on each nanobox can be tailored by controlling the molar ratio of HCl to Ag. Figure 2C shows the structure with multiple attached solid particles on each hollow nanobox prepared from the GRR at a ratio of HCl/Ag = 4:1 (Figure S4). By carefully surveying more than 500 nanoparticles for each sample, we plotted the average number of attached particles on each nanobox as a function of the molar ratio of HCl to Ag (Figure S4E). A clear trend was observed: with the increase of the ratio of HCl to Ag, the number of attached particles increases. After being washed with NaCl and $Fe(NO_3)_3$ solutions, the attached solid particles on each nanobox became hollow; the original heterodimers and multimers were converted to nanostructures with two or multiple hollow domains, while the wall thickness of the cubic part reduced to 2 nm (Figure 2D,E).

To understand the formation of attached particles on nanoboxes, we carefully analyzed the composition of the dimers. X-ray diffraction (XRD) pattern of the as-prepared heterodimers revealed two sets of reflection peaks: one set corresponds to AgCl, and the other set is located between the reflections of Pt and Ag, corresponding to Pt/Ag alloy (Figure S5a). The presence of both Pt/Ag alloy and AgCl in the heterodimers was also confirmed from EDX line scan. Figure 3A shows the composition line profile of an as-prepared dimer. Both Pt and Ag were found in the hollow box and its attached solid particle. However, while the hollow box has a similar amount of Pt and Ag, the attached solid particle shows more Ag than Pt. In addition to Pt and Ag, Cl is also present in the solid particle. These results indicate that, for each heterodimer, the hollow box is mainly composed of Pt/Ag alloy, while the attached solid particle contains both Pt/Ag alloy and AgCl. The presence of Pt/Ag alloy and AgCl in the as-synthesized Pt/Ag dimers was also confirmed from X-ray photoelectron spectroscopy (XPS) analysis, as shown in Figure S6. After being washed with saturated NaCl solution, XRD peaks of AgCl disappeared completely (Figure S5b). Further washing with $Fe(NO_3)_3$ caused the XRD peaks to shift toward Pt due to the dealloying and partial removal of Ag (Figure S5c). At this stage, both hollow domains of the heterodimers are mainly composed of Pt/Ag alloy (Figure 3B). Figure 3C,D shows the lattice fringes of the two hollow domains after washing. Since the *d* spacings of Pt and Ag(111) planes are 0.226 and 0.236 nm, respectively, the 0.229 nm *d* spacing measured for the dimer can be indexed as (111) planes of the Pt/Ag alloy. It is worth mentioning that, due to the presence of Ag in the attached particles before washing with $Fe(NO_3)_3$, one can expect that by reacting the dimers or multimers with another noble metal ions, such as $AuCl_4^-$, Ag can be further dissolved from the dimers to form higher-order hybrid nanostructures. Figure 3E,F shows that, after the GRR between heterodimers and $HAuCl_4$, Au particles were formed on the surface of the attached solid particles. Small Au nanoparticles on Pt have proven to be effective at improving the stability and

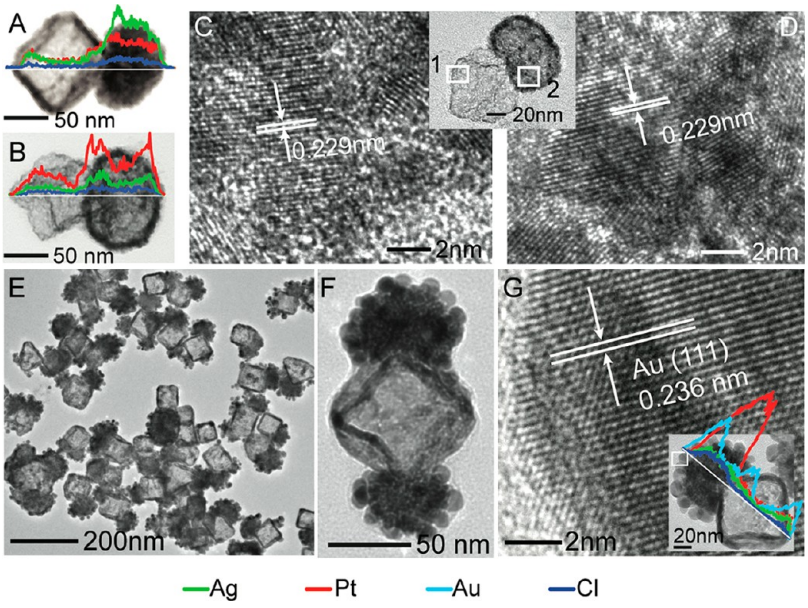

Figure 3. (A,B) EDX line profiles of the Pt/Ag heterodimers before and after being washed with NaCl and $Fe(NO_3)_3$ solutions, respectively. (C,D) HRTEM images of the two hollow domains (indicated by 1 and 2, respectively) of a Pt/Ag dimer after being washed. (E,F) After reacting with $HAuCl_4$, the remaining Ag in Pt/Ag dimers or multimers can be converted to Au to form Au/Pt/Ag hybrid structures. (G) HRTEM and EDX line profile of a Au/Pt/Ag dimer showing the presence of Au.

activity of catalytic oxygen reduction reaction.[40] This type of hybrid structures should be interesting for the study of electrochemical catalysis.

On the basis of the above structural and compositional analyses, we propose the following mechanism for the growth of the attached particles on Pt/Ag nanoboxes. At the initial stage of the reaction between Ag NCs and Pt precursor, due to the presence of an excess amount of Cl^-, AgCl is generated instantaneously once K_2PtCl_4 is introduced in the reaction. AgCl grows and forms islands on the surface of the Ag NCs. Therefore, Pt atoms formed from the reduction by Ag deposit not only onto the surface of Ag NCs but also on the attached AgCl islands. With the consumption of Ag, more Ag atoms migrate from the core to the surface of the nanocube to react with Pt precursor. Ag atoms can also diffuse through the AgCl islands and reach their surface to either form alloy with Pt or react with K_2PtCl_4 to give AgCl. Therefore, the islands swell quickly because of the accumulation of both Pt/Ag alloy and AgCl. The corners and edges of the Ag NCs are especially favored for the nucleation of AgCl due to the surface roughness and more defects of these sites.[41] At relatively low concentration of HCl, AgCl tends to nucleate and grow at one defect site. When HCl at high concentration is added to the reaction, the nucleation of AgCl may occur at multiple defect sites since AgCl is generated at a higher rate. It is worth noting that, in addition to the templating effect, other factors such as surface-adsorbed species may also play a role. Recently, Tao *et al.* showed that positive and negative polyelectrolyte layers on the Ag nanoparticles controlled the GRR with $HAuCl_4$ to obtain different morphologies.[42] When both PVP and HCl are added to the dispersion of Ag NCs, the surface energy of the Ag NCs is changed due to the adsorbed PVP. Therefore, the nucleation and growth of AgCl take place differently, leading to a relatively uniform growth of Pt on the whole surface of Ag NCs to form nanoboxes.

As discussed earlier, the effect of HCl on the synthesis of dimeric or multimeric nanostructures is twofold: (i) to provide a template composed of AgCl for the growth of Pt and (ii) to regulate the reaction kinetic and thus the number of deposition sites. Therefore, if HCl is added to the reaction gradually, a different deposition pattern of AgCl, and thus a different morphology of the resulting Pt/Ag structures, is expected. Indeed, when the reaction was carried out by injecting a mixed solution of HCl and K_2PtCl_4 to the dispersion of Ag NCs, we obtained popcorn-shaped nanoparticles (following reaction route in Figure 1D). Figure 4A,B shows the nanopopcorns formed using 50 nm Ag nanocubes after being washed with NaCl and $Fe(NO_3)_3$ solutions. The average size of the popcorns is 90 nm. Each nanopopcorn is composed of a number of connected hollow particles (average number = 14) with an average wall thickness of 1.7 nm. HRTEM image (Figure 4D) and EDX line profile (Figure 4E) indicate that the popcorn-shaped nanostructures are mainly composed of Pt/Ag alloy.

It is expected that, for the Pt/Ag dimers and popcorns, the presence of multiple hollow interiors and highly porous walls possesses high specific surface area favoring electrochemical catalysis. Therefore, we tested the hollow nanostructures for methanol

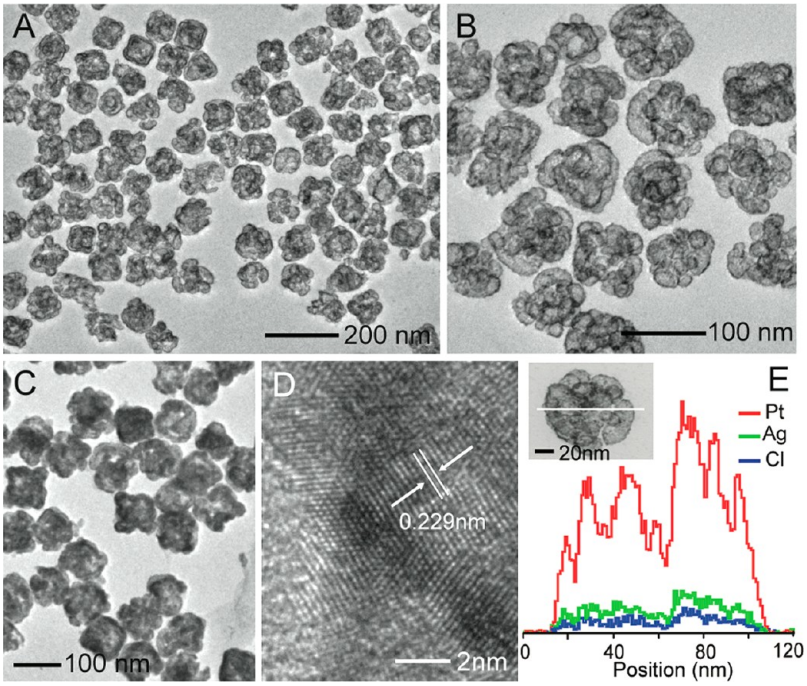

Figure 4. (A) TEM images of Pt/Ag popcorn-shaped nanostructures (A,B) after and (C) before being washed with solutions of saturated NaCl and 50 mM $Fe(NO_3)_3$. (D) HRTEM image and (E) EDX line profile of a Pt/Ag nanopopcorn.

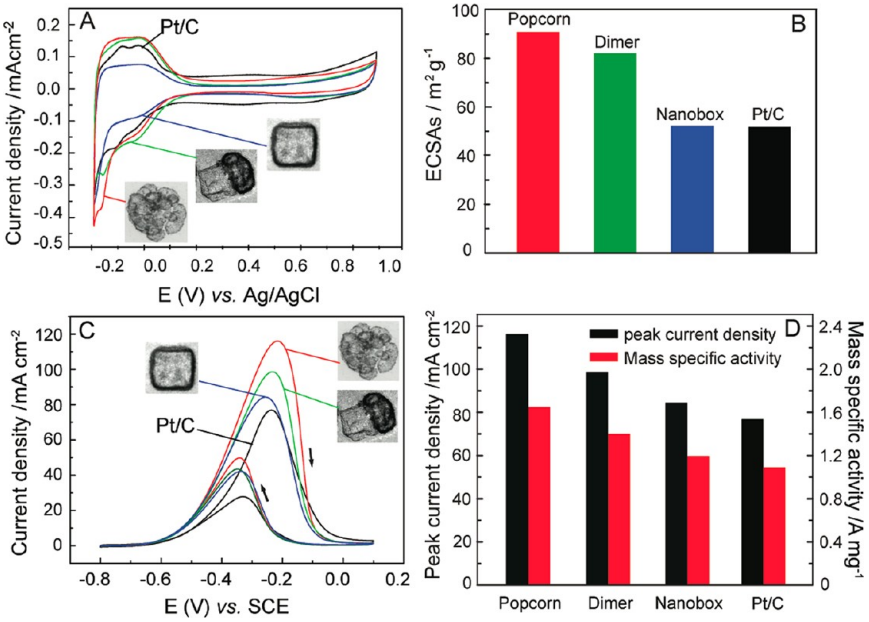

Figure 5. (A) Cyclic voltammograms (CVs) of Pt/C, Pt/Ag hollow nanoboxes, dimers, and popcorns in 1 M $HClO_4$. (B) ECSA of each catalyst. (C) CVs for MOR in a solution containing 1 M CH_3OH and 1 M KOH. (D) Mass activity of each catalyst. The scan rate for all CVs is 50 mV s^{-1}.

oxidation reactions (MOR) and compared their catalytic activities with commercial Pt/C (20 wt %) catalyst with an average diameter of 3.2 nm (based on TEM shown in Figure S11). Figure 5A shows the cyclic voltammograms (CVs) of Pt/Ag popcorns, dimers, nanoboxes, and Pt/C recorded in 1 M $HClO_4$. On the basis of the charge of hydrogen adsorption, the electrochemically activated surface areas (ECSAs) were calculated. For Pt/Ag popcorns, dimers, hollow boxes, and Pt/C, their ECSAs are 90.86, 82.09, 52.19, and 51.81 m^2/g, respectively (Figure 5B). As expected, Pt/Ag dimers and popcorns have much higher ECSAs than that of Pt/C. MORs were performed at room temperature in a solution containing 1 M KOH and 1 M CH_3OH (Figure 5C). For the four samples, the peak current densities decrease in the following order: Pt/Ag

popcorns [116.1 mA cm^{-2}] > dimers [98.6 mA cm^{-2}] > nanoboxes [84.2 mA cm^{-2}] > Pt/C [76.9 mA cm^{-2}]. It is obvious that Pt/Ag popcorns and dimers exhibit improved MOR activities relative to commercial Pt/C (51 and 28% higher, respectively). On the basis of the loading of Pt on the electrode, the mass specific activities of the Pt/Ag nanostructures were calculated and plotted in Figure 5D. It is worth noting that the ECSA and MOR activity of our Pt/Ag nanostructures is competitive compared to existing Pt nanostructures (*e.g.*, ultrathin Pt nanowires with an ECSA of 71.34 m^2 g^{-1} and a MOR mass specific activity 18% higher than commercial Pt/C).[43] To evaluate the stability of the Pt/Ag catalysts, we performed chronoamperometry (CA) measurements at a constant potential of −0.4 V *vs* SCE. As shown in Figure S12, Pt/Ag dimers, nanopopcorns, and nanoboxes exhibited better stability than Pt/C.

CONCLUSIONS

Distinct Pt/Ag hollow nanostructures with controlled number of voids have been synthesized *via* GRR between Ag NCs and K_2PtCl_4 in the presence of HCl. The use of HCl allows the deposition of AgCl on the surface of Ag NCs to regulate the growth of Pt. It is demonstrated that the number of deposition sites for AgCl can be effectively controlled by the amount of HCl. On the basis of this strategy, GRR has been successfully extended to the preparation of bimetallic dimers, multimers, and popcorn-shaped nanostructures. These novel nanostructures with high surface area should be promising for electrochemical catalysis.

METHODS

Materials. Ethylene glycol (EG, J.T. Baker), silver nitrate ($AgNO_3$, Sigma-Aldrich), polyvinylpyrrolidone (PVP, Aldrich $M_w \approx 55\,000$), hydrochloric acid (HCl, Fisher, 37.5%), sodium chloride (NaCl, Sigma-Aldrich), potassium tetrachloroplatinate(II) (K_2PtCl_4, Aldrich), iron(III) nitrate nonahydrate ($Fe(NO_3)_3 \cdot 9H_2O$, Alfa Aesar), isopropyl alcohol (Merck, reagent grade), methanol (Merck, analysis grade), perchloric acid ($HClO_4$, Sigma-Aldrich), potassium hydroxide (KOH, Sigma-Aldrich), and nafion (Sigma-Aldrich, 5% in a mixture of lower aliphatic alcohols and water) were used as received. Ultrapure deionized (DI) water (18.2 MΩ·cm) was used in all experiments. K_2PtCl_4 (5 mM) solutions were aged at least for 24 h before use.

Characterization. Transmission electron microscopy (TEM) images, high-resolution TEM (HRTEM) images, and energy-dispersive X-ray spectroscopy (EDX) spectra were acquired using a JEOL JEM-2100F operating at 200 kV. The X-ray diffraction (XRD) spectra were acquired using a Bruker D8 Advance diffractometer equipped with a Cu Kα radiation source (λ = 1.5418 Å) from samples deposited onto glass substrates. Inductively coupled plasma mass spectrometry (ICP-MS) measurements were carried out with an Agilent 7500 ICP-MS instrument. ICP-MS samples were prepared by dissolving the nanoparticles using fresh aqua regia. The resultant solution was diluted using ultrapure deionized water.

Synthesis of Ag Nanocubes (NCs). Silver NCs (50−70 nm in edge length) were synthesized by a modified polyol process.[44] In a typical synthesis, 10 mL of EG was added into a 50 mL flask and heated under magnetic stirring at 140 °C for 1 h. HCl (2.1 mL, 3.016 mM in EG) was quickly injected into the heated EG using pipet and continued heating for 10 min. $AgNO_3$ (6 mL, 94 mM in EG) and PVP (6 mL, 147 mM in EG) were simultaneously injected into the reaction mixture using a two-channel syringe pump at a rate of 0.6 mL/min. This reaction mixture was allowed to react for around 24−36 h at a temperature of 140 °C with constant stirring. Subsequently, the reaction was removed from the oil bath and quenched in an ice−water bath. The product was mixed with equal volume acetone and centrifuged, followed by washing with water five times to remove the excess PVP. The resultant NCs were dispersed in 20 mL of water in a reaction vial that was wrapped with aluminum foil and stored in a dark cabinet for further use.

Synthesis of Pt/Ag Heterodimers. In a typical synthesis of Pt/Ag heterodimers, a 0.1 mL dispersion of Ag nanocubes (the concentration of Ag is 8.0 mM based on ICP-MS measurement) was added to 4.9 mL of ultrapure deionized water. Then, 0.23 mL of 10 mM HCl was added to the reaction mixture (molar ratio HCl. Ag = 2.75:1). The vial was then heated in an oil bath at 100 °C for 5 min. Then, 0.5 mL of 5 mM K_2PtCl_4 solution was injected into the reaction mixture using a syringe pump at a rate of 1 mL/min. The reaction mixture was continually stirred and heated at 100 °C until no further color change (about 5 min). The reaction mixture was centrifuged and washed using saturated NaCl, 50 mM $Fe(NO_3)_3$, and water to remove AgCl, Ag, and residual ions, respectively. The final product was dispersed in 1.0 mL of DI water.

Synthesis of Au/Ag Heterodimers. For Au/Ag dimers, the procedure was identical to that of Pt/Ag dimers, except that 0.4 mL of 0.5 mM $HAuCl_4$ solution was injected into the dispersion of Ag NCs in the presence of HCl.

Synthesis of Pt/Ag Nanoboxes. A synthetic approach similar to Pt/Ag dimers was followed for Pt/Ag hollow nanoboxes, except that 0.5 mL of PVP solution (100 mM) was added to the mixture of HCl and Ag NCs prior to the injection of K_2PtCl_4 solution.

Synthesis of Au/Pt/Ag Structures. One milliliter of Pt/Ag heterodimers (without being washed with $Fe(NO_3)_3$ solution) was dispersed in 4.0 mL of DI H_2O. The vial was then heated at 100 °C for 5 min. Then, 0.1 mL of $HAuCl_4$ solution (0.5 mM) was injected into the reaction mixture using a syringe pump at a rate of 0.2 mL/min. The reaction mixture was continually stirred and heated at 100 °C for another 5 min. After being washed, the product was dispersed in 0.5 mL of DI water.

Synthesis of Pt/Ag Popcorn-Shaped Nanostructures. First, 0.5 mL of 10 mM HCl was mixed with 0.5 mL of 5 mM K_2PtCl_4 for 2 h. Then, 0.5 mL of 100 mM PVP was added to the dispersion of Ag NCs, and the solution was heated for 5 min in the oil bath before the injection of the solution containing K_2PtCl_4 and HCl at a rate of 2 mL/min. The reaction mixture was centrifuged and washed using saturated NaCl, 50 mM $Fe(NO_3)_3$, and water to remove AgCl, Ag, and residual ions, respectively. The final product was dispersed in 1.0 mL of DI water.

Electrochemical Analysis. Electrochemical measurements for the Pt/Ag nanoparticles were carried out by cyclic voltammetry using a potentiostat (BioLogic Science Instruments, VSP Modular 5 Channels). The cell was assembled as a three-electrode setup consisting of a glass carbon electrode (GCE) as the working electrode, Pt wire as the counter electrode, and saturated calomel electrode as the reference electrode. Pt/Ag catalyst ink was prepared by dispersing the nanoparticles into 200 μL of 20% isopropyl alcohol in water solution. From ICP-MS measurements, the concentrations of Pt for Pt/Ag popcorns, dimers, and hollow nanoboxes were 960, 609, 778 ppm, respectively. The molar ratios of Pt to Ag for the three samples are listed in Table S1 (Supporting Information). Specific volume of these catalysts was then dropped on the GC electrode (3 mm diameter, 0.071 cm^2). Commercial E-Tek Pt/C catalyst (Pt loading: 20 wt %) was used as the reference. For all catalysts, the loading of Pt was 5 μg. After drying of the catalyst, 5 μL of 0.1 wt % nafion

solution (diluted from 5% Nafion with ethanol) was dropped onto the electrode and dried in air. Electrochemical surface area (ECSA) for the nanoparticles was measured in 1 M $HClO_4$ solution. Methanol oxidation catalytic activity of the nanoparticles was measured in a solution containing 1 M KOH and 1 M CH_3OH. The sweep rate of all measurements was 50 mV s^{-1}. Chronoamperometry experiments were conducted by monitoring current at the potential constant at −0.4 V *vs* SCE in a solution containing 1 M KOH and 1 M CH_3OH.

Conflict of Interest: The authors declare no competing financial interest.

Acknowledgment. We are thankful for the financial support from Ministry of Education, Singapore, under research projects R279-000-298-112/273-133.

Supporting Information Available: Additional characterization data including TEM images, XRD, EDX, XPS, UV−vis, chronoamperometry measurements, and calculation of ECSA. This material is available free of charge *via* the Internet at http://pubs.acs.org.

REFERENCES AND NOTES

1. Sun, Y.; Xia, Y. Shape-Controlled Synthesis of Gold and Silver Nanoparticles. *Science* **2002**, *298*, 2176–2179.
2. Skrabalak, S. E.; Chen, J.; Sun, Y.; Lu, X.; Au, L.; Cobley, C. M.; Xia, Y. Gold Nanocages: Synthesis, Properties, and Applications. *Acc. Chem. Res.* **2008**, *41*, 1587–1595.
3. Cobley, C. M.; Xia, Y. Engineering the Properties of Metal Nanostructures *via* Galvanic Replacement Reactions. *Mater. Sci. Eng., R* **2010**, *70*, 44–62.
4. Skrabalak, S. E.; Au, L.; Lu, X.; Li, X.; Xia, Y. Gold Nanocages for Cancer Detection and Treatment. *Nanomedicine* **2007**, *2*, 657–668.
5. Xu, C.; Li, Y.; Tian, F.; Ding, Y. Dealloying to Nanoporous Silver and Its Implementation as a Template Material for Construction of Nanotubular Mesoporous Bimetallic Nanostructures. *ChemPhysChem* **2010**, *11*, 3320–3328.
6. Seo, D.; Song, H. Asymmetric Hollow Nanorod Formation through a Partial Galvanic Replacement Reaction. *J. Am. Chem. Soc.* **2009**, *131*, 18210–18211.
7. Sun, Y.; Xia, Y. Mechanistic Study on the Replacement Reaction between Silver Nanostructures and Chloroauric Acid in Aqueous Medium. *J. Am. Chem. Soc.* **2004**, *126*, 3892–3901.
8. Lu, X.; Tuan, H.-Y.; Chen, J.; Li, Z.-Y.; Korgel, B. A.; Xia, Y. Mechanistic Studies on the Galvanic Replacement Reaction between Multiply Twinned Particles of Ag and $HAuCl_4$ in an Organic Medium. *J. Am. Chem. Soc.* **2007**, *129*, 1733–1742.
9. Tan, Y. N.; Yang, J.; Lee, J. Y.; Wang, D. I. C. Mechanistic Study on the Bis(*p*-sulfonatophenyl)phenylphosphine Synthesis of Monometallic Pt Hollow Nanoboxes Using Ag*−Pt Core−Shell Nanocubes as Sacrificial Templates. *J. Phys. Chem. C* **2007**, *111*, 14084–14090.
10. Huang, X.; Zhang, H.; Guo, C.; Zhou, Z.; Zheng, N. Simplifying the Creation of Hollow Metallic Nanostructures: One-Pot Synthesis of Hollow Palladium/Platinum Single-Crystalline Nanocubes. *Angew. Chem., Int. Ed.* **2009**, *48*, 4808–4812.
11. Skrabalak, S. E.; Au, L.; Li, X.; Xia, Y. Facile Synthesis of Ag Nanocubes and Au Nanocages. *Nat. Protoc.* **2007**, *2*, 2182–2190.
12. Sun, Y.; Mayers, B.; Xia, Y. Metal Nanostructures with Hollow Interiors. *Adv. Mater.* **2003**, *15*, 641–646.
13. Sun, Y.; Wiley, B.; Li, Z. Y.; Xia, Y. Synthesis and Optical Properties of Nanorattles and Multiple-Walled Nanoshells/Nanotubes Made of Metal Alloys. *J. Am. Chem. Soc.* **2004**, *126*, 9399–9406.
14. Lu, X.; Au, L.; McLellan, J.; Li, Z.-Y.; Marquez, M.; Xia, Y. Fabrication of Cubic Nanocages and Nanoframes by Dealloying Au/Ag Alloy Nanoboxes with an Aqueous Etchant Based on $Fe(NO_3)_3$ or NH_4Oh. *Nano Lett.* **2007**, *7*, 1764–1769.
15. Chen, X.; Cui, C.-H.; Guo, Z.; Liu, J.-H.; Huang, X.-J.; Yu, S.-H. Unique Heterogeneous Silver−Copper Dendrites with a Trace Amount of Uniformly Distributed Elemental Cu and Their Enhanced SERS Properties. *Small* **2011**, *7*, 858–863.
16. Huang, J.; Vongehr, S.; Tang, S.; Lu, H.; Meng, X. Highly Catalytic Pd−Ag Bimetallic Dendrites. *J. Phys. Chem. C* **2010**, *114*, 15005–15010.
17. Yin, Y.; Erdonmez, C.; Aloni, S.; Alivisatos, A. P. Faceting of Nanocrystals during Chemical Transformation: From Solid Silver Spheres to Hollow Gold Octahedra. *J. Am. Chem. Soc.* **2006**, *128*, 12671–12673.
18. Lu, X.; McKiernan, M.; Peng, Z.; Lee, E. P.; Yang, H.; Xia, Y. Noble-Metal Nanotubes Prepared *via* a Galvanic Replacement Reaction between Cu Nanowires and Aqueous $HAuCl_4$, H_2PtCl_6, or Na_2PdCl_4. *Sci. Adv. Mater.* **2010**, *2*, 413–420.
19. Chen, J.; Wiley, B.; McLellan, J.; Xiong, Y.; Li, Z.-Y.; Xia, Y. Optical Properties of Pd−Ag and Pt−Ag Nanoboxes Synthesized *via* Galvanic Replacement Reactions. *Nano Lett.* **2005**, *5*, 2058–2062.
20. Yin, A.-X.; Min, X.-Q.; Zhu, W.; Liu, W.-C.; Zhang, Y.-W.; Yan, C.-H. Pt−Cu and Pt−Pd−Cu Concave Nanocubes with High-Index Facets and Superior Electrocatalytic Activity. *Chem.—Eur. J.* **2011**, *18*, 777–782.
21. Zhang, H.; Jin, M.; Wang, J.; Li, W.; Camargo, P. H. C.; Kim, M. J.; Yang, D.; Xie, Z.; Xia, Y. Synthesis of Pd−Pt Bimetallic Nanocrystals with a Concave Structure through a Bromide-Induced Galvanic Replacement Reaction. *J. Am. Chem. Soc.* **2011**, *133*, 6078–6089.
22. Zhang, G.; Sun, S.; Li, R.; Sun, X. New Insight into the Conventional Replacement Reaction for the Large-Scale Synthesis of Various Metal Nanostructures and Their Formation Mechanism. *Chem.—Eur. J.* **2010**, *16*, 10630–10634.
23. Niu, K.-Y.; Kulinich, S. A.; Yang, J.; Zhu, A. L.; Du, X.-W. Galvanic Replacement Reactions of Active-Metal Nanoparticles. *Chem.—Eur. J.* **2012**, *18*, 4234–4241.
24. Chen, J.; Saeki, F.; Wiley, B. J.; Cang, H.; Cobb, M. J.; Li, Z.-Y.; Au, L.; Zhang, H.; Kimmey, M. B.; Li, X.; *et al.* Gold Nanocages: Bioconjugation and Their Potential Use as Optical Imaging Contrast Agents. *Nano Lett.* **2005**, *5*, 473–477.
25. Chen, J.; Wang, D.; Xi, J.; Au, L.; Siekkinen, A.; Warsen, A.; Li, Z.-Y.; Zhang, H.; Xia, Y.; Li, X. Immuno Gold Nanocages with Tailored Optical Properties for Targeted Photothermal Destruction of Cancer Cells. *Nano Lett.* **2007**, *7*, 1318–1322.
26. Yavuz, M. S.; Cheng, Y.; Chen, J.; Cobley, C. M.; Zhang, Q.; Rycenga, M.; Xie, J.; Kim, C.; Song, K. H.; Schwartz, A. G.; *et al.* Gold Nanocages Covered by Smart Polymers for Controlled Release with Near-Infrared Light. *Nat. Mater.* **2009**, *8*, 935–939.
27. Rycenga, M.; Hou, K. K.; Cobley, C. M.; Schwartz, A. G.; Camargo, P. H. C.; Xia, Y. Probing the Surface-Enhanced Raman Scattering Properties of Au−Ag Nanocages at Two Different Excitation Wavelengths. *Phys. Chem. Chem. Phys.* **2009**, *11*, 5903.
28. Olson, T. Y.; Schwartzberg, A. M.; Orme, C. A.; Talley, C. E.; O'Connell, B.; Zhang, J. Z. Hollow Gold−Silver Double-Shell Nanospheres: Structure, Optical Absorption, and Surface-Enhanced Raman Scattering. *J. Phys. Chem. C* **2008**, *112*, 6319–6329.
29. Feng, Y.-Y.; Zhang, G.-R.; Ma, J.-H.; Liu, G.; Xu, B.-Q. Carbon-Supported Pt/Ag Nanostructures as Cathode Catalysts for Oxygen Reduction Reaction. *Phys. Chem. Chem. Phys.* **2011**, *13*, 3863.
30. Ye, F.; Liu, H.; Hu, W.; Zhong, J.; Chen, Y.; Cao, H.; Yang, J. Heterogeneous Au−Pt Nanostructures with Enhanced Catalytic Activity toward Oxygen Reduction. *Dalton Trans.* **2012**, *41*, 2898.
31. Alia, S. M.; Zhang, G.; Kisailus, D.; Li, D.; Gu, S.; Jensen, K.; Yan, Y. Porous Platinum Nanotubes for Oxygen Reduction and Methanol Oxidation Reactions. *Adv. Funct. Mater.* **2010**, *20*, 3742–3746.
32. Ridelman, Y.; Singh, G.; Popovitz-Biro, R.; Wolf, S. G.; Das, S.; Klajn, R. Metallic Nanobowls by Galvanic Replacement Reaction on Heterodimeric Nanoparticles. *Small* **2012**, *8*, 654–660.

33. Zelyanskii, A. V.; Zhukova, L. V.; Kitaev, G. A. Solubility of AgCl and AgBr in HCl and HBr. *Inorg. Mater.* **2001**, *37*, 523–526.
34. He, W.; Wu, X.; Liu, J.; Zhang, K.; Chu, W.; Feng, L.; Hu, X.; Zhou, W.; Xie, S. Formation of AgPt Alloy Nanoislands *via* Chemical Etching with Tunable Optical and Catalytic Properties. *Langmuir* **2010**, *26*, 4443–4448.
35. Xu, C.; Liu, Y.; Su, F.; Liu, A.; Qiu, H. Nanoporous PtAg and PtCu Alloys with Hollow Ligaments for Enhanced Electrocatalysis and Glucose Biosensing. *Biosens. Bioelectron.* **2011**, *27*, 160–166.
36. Lee, C.-L.; Tseng, C.-M. Ag−Pt Nanoplates: Galvanic Displacement Preparation and Their Applications as Electrocatalysts. *J. Phys. Chem. C* **2008**, *112*, 13342–13345.
37. Mahmoud, M. A.; El-Sayed, M. A. Metallic Double Shell Hollow Nanocages: The Challenges of Their Synthetic Techniques. *Langmuir* **2012**, *28*, 4051–4059.
38. Bi, Y.; Ye, J. Heteroepitaxial Growth of Platinum Nanocrystals on AgCl Nanotubes *via* Galvanic Replacement Reaction. *Chem. Commun.* **2010**, *46*, 1532.
39. Chen, M.; Wu, B.; Yang, J.; Zheng, N. Small Adsorbate-Assisted Shape Control of Pd and Pt Nanocrystals. *Adv. Mater.* **2012**, *24*, 862–879.
40. Zhang, J.; Sasaki, K.; Sutter, E.; Adzic, R. R. Stabilization of Platinum Oxygen-Reduction Electrocatalysts Using Gold Clusters. *Science* **2007**, *315*, 220–222.
41. Sugimoto, T.; Miyake, K. Mechanism of Halide Conversion Process of Colloidal AgCl Microcrystals by Br^- Ions I. Observation of the Dynamic Changes in Shape, Structure, and Composition. *J. Colloid Interface Sci.* **1990**, *140*, 335–347.
42. Hsu, S.-W.; On, K.; Gao, B.; Tao, A. R. Polyelectrolyte-Templated Synthesis of Bimetallic Nanoparticles. *Langmuir* **2011**, *27*, 8494–8499.
43. Zhang, L.; Li, N.; Gao, F.; Hou, L.; Xu, Z. Insulin Amyloid Fibrils: An Excellent Platform for Controlled Synthesis of Ultrathin Superlong Platinum Nanowires with High Electrocatalytic Activity. *J. Am. Chem. Soc.* **2012**, *134*, 11326–11329.
44. Im, S. H.; Lee, Y. T.; Wiley, B.; Xia, Y. Large-Scale Synthesis of Silver Nanocubes: The Role of HCl in Promoting Cube Perfection and Monodispersity. *Angew. Chem., Int. Ed.* **2005**, *44*, 2154–2157.